

Received September 15, 2021, accepted December 8, 2021, date of publication December 10, 2021, date of current version December 29, 2021.

Digital Object Identifier 10.1109/ACCESS.2021.3134887

Locally Aligned Image Stitching Based on Multi-Feature and Super-Pixel Segmentation With Plane Protection

JIALIANG LI^{1,2}, DONG WU¹, PINQUN JIANG², ZILI LI^{1,2}, AND SHUXIANG SONG²

¹College of Artificial Intelligence, Zhejiang Post and Telecommunication College, Shaoxing, Zhejiang 312366, China

²College of Electronic Engineering, Guangxi Normal University, Guilin 541004, China

Corresponding authors: Jialiang Li (ljliang@zptc.edu.cn) and Zili Li (zlienishi@mailbox.gxnu.edu.cn)


This work was supported in part by the National Natural Science Foundation of China under Grant 11465004 and Grant 61402491, in part by the Guilin Scientific Research and Technology Development Plan Project under Grant 20170113-4, in part by the Project of Zhejiang Polytechnic of Posts and telecommunications in 2021 under Grant KY202112, and in part by the General Scientific Research Project of Zhejiang Provincial Department of Education under Grant Y202148210.

ABSTRACT The number and accuracy of image feature matching directly affect the accuracy of image warping, which is gaining widespread attention in image stitching. The alignment accuracy is gradually improved from a single plane to a regular multi-plane warping model. To further improve the accuracy of image alignment, this paper proposes a multi-plane alignment method based on superpixel segmentation, which preserves the integrity of local planes as much as possible to reduce ghosting. Recent warps prove that line features provide strong correspondences, especially in low-textured cases. Moreover, image segmentation methods such as superpixel segmentation have the function of protecting the object's integrity. On the one hand, our approach is based on GMS matching and introduces superpixel segmentation to refine the matching in the feature matching stage. The homography combines line features to enrich as many matching points as possible. On the other hand, to solve the problem of misalignment caused by local warping, the proposed method makes full use of the characteristics of superpixels to perform irregular plane segmentation to avoid the traditional rectangular segmentation method from dividing different planes into the same grid. Experimental results demonstrate that the proposed method outperforms some state-of-the-art warps from both qualitative and quantitative aspects, including the as-projective-as-possible warp (APAP), the as-natural-as-possible warp (ANAP), the global similarity prior (GSP), etc.

INDEX TERMS Image stitching, image segmentation, local warping, image alignment.

I. INTRODUCTION

Image stitching, which is widely used in video surveillance [1], panorama [2], [3], virtual reality [4], [5], and other fields of technology, is an important research area in the past few decades [6]. It can combine multiple images into a single wide-angle panorama through the critical process of alignment and blending [7]. Multi-homography, calculated by matching and mesh-based warping [8], transforms the image to the same coordinate system to complete local alignment [9]. Image blending, the process is to apply reasonable weighting coefficients in the overlapping area, adjust the pixel intensity to achieve a smooth transition of the image.

The associate editor coordinating the review of this manuscript and approving it for publication was Gianluigi Ciocca .

Earlier, the warps directly stack the homography, a commonly used warping model due to the flexibility of its plane transformation, gradually improving the local alignment ability. The global warps represented by AutoStitch [10] are devoted to minimizing the projection deviation between overlapping positions by iterating a global transformation. This method is perfect only when the scene is coplanar. The spatially-varying warps [11]–[14] based on multiple transformations weighted by relative positions replace the single global transformation to address the problem of misalignment in overlapping regions. These methods perform rectangular segmentation on the image and calculate the local transformation relationship based on the position correlation, which improves the alignment accuracy to a certain extent. However, limited to segmentation methods, these methods

still have the problem of misalignment in overlapping regions (see Figure 1(b)). What is more, the distortion of the non-overlapping region is also a challenge in scenes with large parallax.

Later, the warps focus on obtaining more natural stitched images [15]–[17]. The mainstream method introduces similarity to reduce distortion caused by viewing angle changes [18]. The method of improving the naturalness of the image by introducing corresponding constraints (mainly line features [19], [20]) is also popular [21]–[23]. Because the line feature can provide excellent and reliable local geometric correspondence, even in low-texture scenes such as white walls. Not only that, the warping method based on seam driving and constraint terms can effectively solve the artifact like ghosting caused by parallax without relying on high-alignment accuracy models [24]–[26]. Alignment accuracy and distortion are still challenging in large parallax scenarios for these methods (see Figure 1(c)).

Recently, the warps [27], [28] with deviation correction based on the thin-plate spline [29], [30] have effectively improved the alignment effect. Moreover, the optimized warping for the homography model [9], [31] effectively solves the distortion problem caused by the change of viewing angle. Moreover, reasonable meshing to adapt to the coplanar characteristics of homography can also achieve better visual effects [32], [33]. The warps have achieved considerable splicing results, but they are difficult to cope with complex scenes (see Figure 1(e)).

This paper proposes a multi-plane alignment method based on superpixel segmentation to overcome the drawback of image misalignment in existing stitching methods. Different from our previous work [28] that obtains the aligned image by correcting the projection deviation (see Figure 1(d)), this paper uses appropriate image segmentation to make the image cell fit the ideal condition of coplanarity as much as possible to improve the alignment ability. Not only that, line features are introduced into the feature matching stage of the image to enrich the number of features. They are used as an auxiliary means to improve the accuracy of image alignment. Our proposed warping creates a precisely aligned mosaic (see Figure 1(f)).

To summarize our contribution:

1) We introduce line features that can be regarded as an effective supplement to point features to enrich image matching. Because, in most scenes, line features are relatively rich, which can provide rich correspondences for accurate distortion model estimation. In addition, compared to feature points, line features have more stable geometric information, which is conducive to creating a more natural-looking mosaic.

2) We introduce superpixel segmentation in the feature matching and local warping stages. The proposed method protects the integrity of image cells. Specifically, image segmentation is helpful to feature matching by classifying features according to their respective planes. In addition, irregular plane segmentation can effectively avoid the hetero-

geneous objects sticking in the same image cell, and fit the homography coplanar condition as much as possible.

The rest of this paper is organized as follows. Section II briefly describes important works. Section III gives our approach in detail, which is a multi-plane alignment method based on superpixel segmentation. Experimental results and comparisons with other methods are shown in Section IV. Finally, the conclusion of our work is drawn in Section V.

II. RELATED WORK

The algorithm for stitching images has been well studied, and a comprehensive survey about it can be found in [6] and [34]. Feature matching and image alignment are two critical processes of image stitching. This section reviews some important works of image stitching in feature matching and image alignment.

A. FEATURE MATCHING

Scale Invariant Feature Transform (SIFT) [35], Speeded Up Robust Features (SURF) [36], and Oriented fast and Rotated Brief (ORB) [37] are representative algorithms for early feature point matching. Lowe used the Gaussian model to differential pyramid image and constructed a 128-dimensional feature descriptor. Bay *et al.* introduced box filter and integral graph to accelerate SIFT, while Rublee introduced pyramid image and centroid algorithm based on the Features from Accelerated Segment Test (FAST) [38] to propose a faster feature detection and matching algorithm. Bian *et al.* [39] proposed a grid-based motion Statistics (GMS) algorithm based on assuming that adjacent pixels in an image will move together. These methods will still cause some mismatches in some scenarios (see Part III).

Line feature is another form of the image feature, which has significant value in the field of vision. Earlier research, such as Line Segment Detector (LSD) [19] based on pixel gradient, led to the fragmentation of straight lines. Zhang *et al.* [20] proposed the introduction of the Gaussian pyramid to construct Line Band Descriptor (LBD), which enhanced the scale invariance of line matching. Recently, Jia *et al.* [40] proposed Coplanar Line-Points Invariants based on LSD to improve the tolerance of line matching to low texture and parallax. Li *et al.* [41] proposed hierarchical line matching by constructing Line-Junction-Line in multi-scale pyramid images. Line features have strong geometric constraints for image alignment, but few studies integrate line features into feature matching to improve image alignment accuracy.

B. IMAGE ALIGNMENT

After the feature matching is completed, the warping is constructed through the corresponding relationship of the features to achieve image alignment.

Early warping focused on global alignment [10]–[12], and this solution is effective only under the assumption that the input images are roughly coplanar (i.e., the scene depth difference is small). The global warp is robust but lacks flexibility and is difficult to provide accurate alignment.



FIGURE 1. Stitching images with large parallax. (a) Input images. (b) to (f) are the stitched images of APAP [13], ANAP [16], AAAP [28], TFA [33], and our approach.

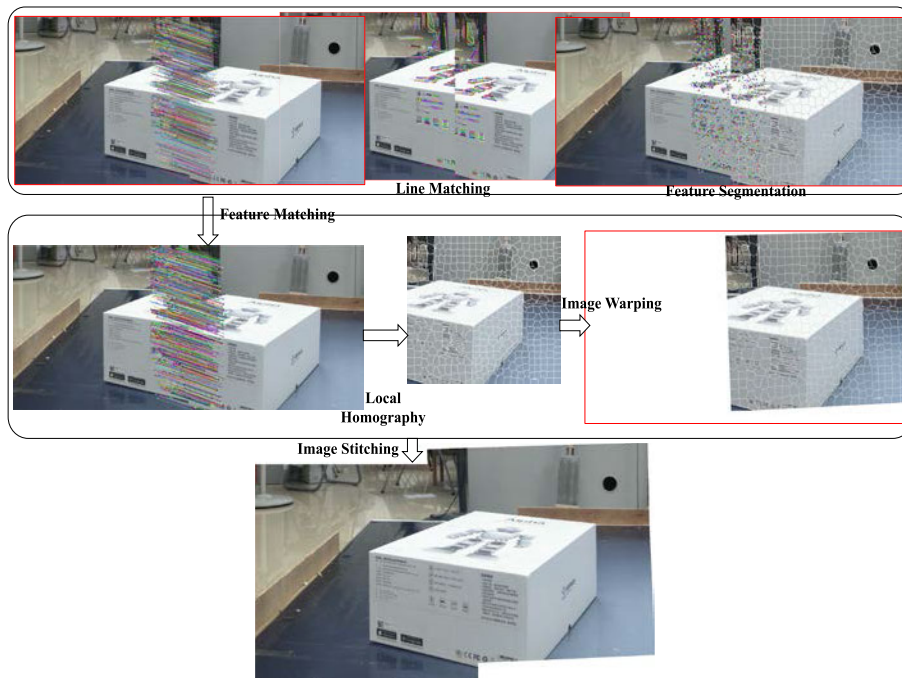
Later, warping focused on the quality of alignment to solve the problems caused by global alignment. The as-projective-as-possible (APAP) warp [13] based on the rectangular grid provides more flexible warping, while other methods ([24], [25], and [42]) dynamically calculate stitched parallax images through the seam-driven method. The APAP uses moving direct linear transformation to assign global homography weights to each grid to achieve local approximation alignment. The stitching method of seam-driven

guidance does not require perfect alignment in the entire overlapping region. However, these methods are still homography warping, which will suffer from perspective distortion without constraints. Correspondingly, introducing constraints is an effective way to improve image alignment. The spatial combination method of homography and similarity is a typical constraint, and the most representative ones are the shape-preserving half-projective (SPHP) warp [15] and the as-natural-as-possible (ANAP) warp [16]. They balance

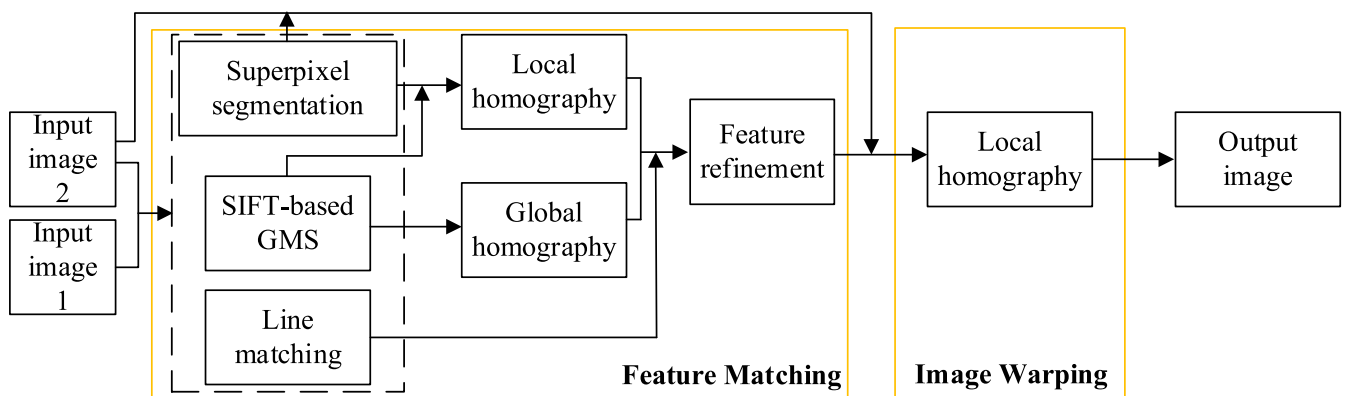
homography and similarity to deal with the distortion caused by perspective. However, the distortion will be amplified for images with a large field of view. Lines can provide more robust correspondences than point matching and can be used as constraints for image alignment. The straight-line constraint is introduced in warping to improve the alignment accuracy of the image in [1], [21]–[23], and [26]. However, the problem of image misalignment still exists.

The recent warps solve the naturalness problem of the image by implementing different constraints. Zhang *et al.* [17] used regular mesh grids to define the energy function, including alignment term, regularization term, scale term, and extra constraint and transformed the image to the same coordinate system to complete the image alignment. The grided global-similarity-prior (GSP) warp [18], which includes alignment

term, local similarity term, and global similarity term, constrains the warp to resemble a whole similarity. Constructing a binary mapping system is also an effective constraint method. Li *et al.* [9] constructed a binary function of slope preservation and scale linearization to describe perspective distortion and projective distortion and proposed the quasi-homography (QH) warp. The single-perspective warp proposed by Liao *et al.* [31] contains two more abundant alignment schemes. One is a combination of dual-feature-based APAP and the quasi-homography warp, and the other is an energy function that integrates alignment term, distortion term, and saliency term. In the previous work, we optimized the feature fine matching, and inspired by [27], we proposed the As-aligned-as-possible (AAP) warp [28] based on the thin-plate spline (TPS) [29] to correct the mapping deviation



(a) Illustration of the overview of the proposed method



(b) Program flowchart

FIGURE 2. Flowchart of the proposed image stitching approach.

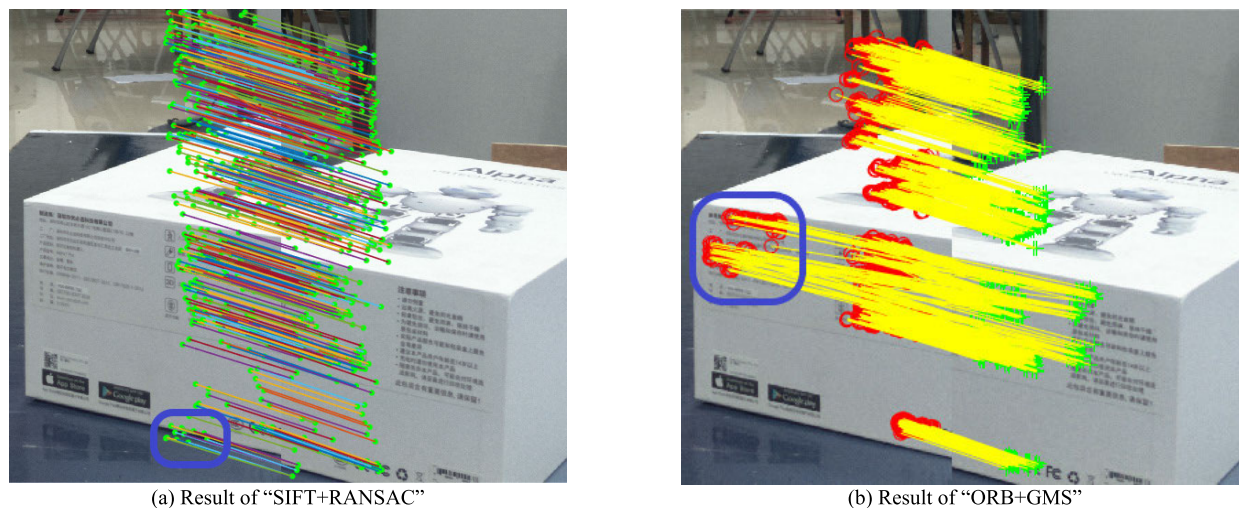


FIGURE 3. Mismatches in advanced matching methods. Rounded rectangles mark obvious mismatch points.

to obtain more accurate stitching of images. In the latest work of Li et al. [33], the scene is approximated as a combination of adjacent triangular facets, and a warping based on the triangular facet approximation (TFA) is proposed.

III. THE PROPOSED APPROACH

The Framework of the Proposed Method: This section describes our proposed approach, which uses a common image stitching pipeline. Figure 2 illustrates the overall process of the proposed method, which mainly consists of two steps. Figure (a) shows the resulting image of each process, and figure (b) illustrates the flow of the proposed method and related algorithms. The first step is a parallel process of multiple algorithms, including point feature matching, line feature matching, and image segmentation based on superpixels. Then, the initial homography is calculated by superpixel constraints to refine the feature set, and the endpoints of the line feature are introduced. In the second step, the APAP-based homography is first updated from the refined features, and then the homography of a specific plane is calculated through the constraints of superpixels. Finally, the estimated homography is used to map the image onto the canvas, and the pixels on the canvas are merged with linear weights to complete the image stitching.

A. RICHER FEATURES

Feature matching is a crucial step in image stitching, which directly determines the quality of the resulting image. At present, even for some advanced matching algorithms, there are still some challenges, as shown in Figure 3. As a result, some wrong matches are kept. Feature richness is another factor affecting feature quality. Therefore, the line features that contain the mapping relationship between images, like the importance of feature points, are also of great significance for image stitching. To enhance the richness of features, we added line features to point features and introduced superpixel segmentation to improve matching

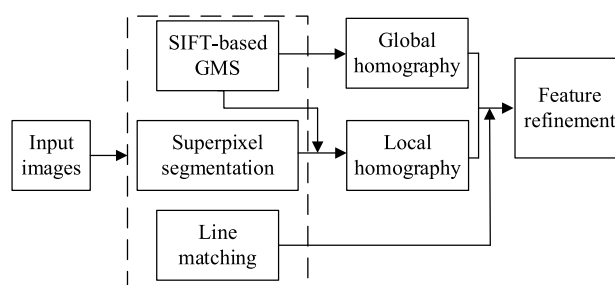


FIGURE 4. Flowchart of matching strategy.

accuracy. The matching strategy is shown in Figure 4. First, algorithms such as point feature, line feature, and superpixel segmentation are executed in parallel. Then the point features are matched to calculate the global homography matrix. And at the same time, the local homography matrix is calculated using plane constraints. Finally, the feature point set (the feature point and the line’s endpoint) is precisely matched to delete the mismatched point.

1) MATCHING OF FEATURES

As shown in Figure 3, SIFT acquires evenly distributed features, while ORB features are too concentrated or sparse. The SIFT descriptor has high stability, and the matching efficiency of the GMS is better than the RANSAC [43]. Therefore, we use SIFT to detect features and then use GMS to perform initial matching of feature points to retain the scale invariance and efficiency of the feature matching algorithm. The SIFT-based GMS matching result is shown in Figure 5, and 1268 pairs of matching feature points are obtained, which took 2.107 seconds (GMS takes less than 0.01 seconds). In Figure 3(a), there are a total of 507 pairs of matching features, which took 4.32 seconds (RANSAC took 2.13 seconds).

However, a few mismatches are still obvious in Figure 5. To this end, we use the feature refinement method based on



FIGURE 5. Matching results of GMS based on SIFT.

normal distribution [28] to eliminate mismatches to calculate the initial homography. That is, the initial matching is used to calculate the global homography, and the local homography is calculated by weighting. Then, the projection error between the feature pairs eliminates the wrong matching. Considering that the homography is limited by the condition of coplanarity, this paper introduces superpixel segmentation to optimize the fine matching of features. Superpixels act on features in a local plane to obtain the true homography of the plane instead of approximating the true homography in a weighted manner. Image segmentation can segment planes to achieve feature classification. The image is divided into planes through the Gaussian Mixture Model (GMM) [44] algorithm, as shown in Figure 6. We know that the feature points are accurately placed in the plane with the image. Therefore, we directly use these points to calculate the exact homography to avoid errors caused by weighting. In particular, when the number of plane feature points is less than four pairs, the weighted homography is used as the plane's homography.

2) INTRODUCTION OF LINE FEATURES

Line features (endpoints of lines) can also be integrated into point sets to enrich feature points. The homography corresponding to each plane can be obtained through the above steps, which provide stability for introducing line features. Therefore, this paper uses precise matching on the endpoints of the line features output by the HLM algorithm and introduces point features in the matching set to enrich the number of features. First, the mapping points corresponding to the endpoints of the line features are calculated by homography. Then, the mapping deviation between the endpoint and the corresponding mapping point is calculated. Finally, set the error range of the mapping deviation. The endpoints whose error is less than the threshold are regarded as matching point pairs and added to the matching set. In particular, it is known from experiments that the error range is within the range of

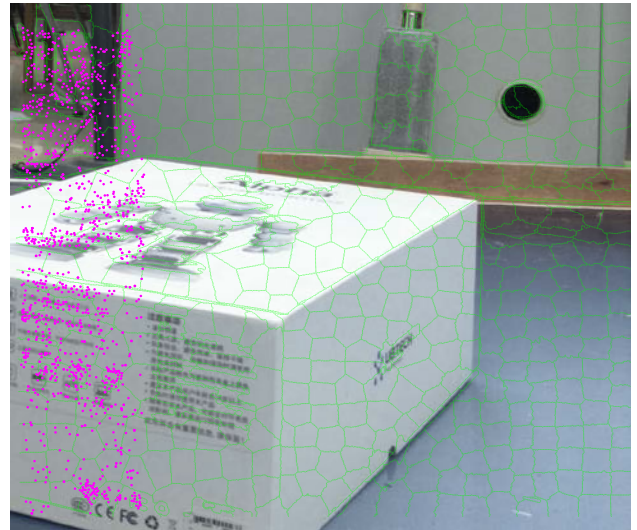


FIGURE 6. Feature distribution under different planes. The purple dots represent matching features, and irregular green graphics represent different planes.



(a) Matched line feature



(b) Matched line end (293 matches)



(c) The final set of matching points

FIGURE 7. The introduction process of line features.

2-10 pixels, and the matching effect of the line endpoints is better.

Figure 7 shows the introduction of line features. The end of the line is a reasonably objective feature, which can

effectively compensate for the number of features and provide a powerful mapping relationship. Compared with the methods in Figure 3 and Figure 5, the proposed method (Figure 7(c)) has more feature points, a more uniform distribution, and more accurate matching.

B. ACCURATE ALIGNMENT

We first review the estimation of local homography commonly used for image stitching and then describe the proposed multi-plane alignment method based on superpixel segmentation.

1) LOCAL HOMOGRAPHY

Let the points $\mathbf{p} = [x, y, 1]^T$ and $\mathbf{q} = [u, v, 1]^T$ denote the matching in the reference image I1 and the target image I2 respectively. The homography \mathbf{H} is estimated by the direct linear transformation (DLT) from the corresponding points, $\mathbf{H} \in \mathbb{R}^{3 \times 3}$, that is

$$\begin{bmatrix} u \\ v \\ 1 \end{bmatrix} \sim \begin{bmatrix} h_{11} & h_{12} & h_{13} \\ h_{21} & h_{22} & h_{23} \\ h_{31} & h_{32} & h_{33} \end{bmatrix} \begin{bmatrix} x \\ y \\ 1 \end{bmatrix} \quad (1)$$

where \sim denotes equality up to a scale factor, h_{ij} is the element of matrix \mathbf{H} .

The homography \mathbf{H} can be expressed as $\mathbf{q} = \mathbf{H}\mathbf{p}$. The columns of \mathbf{H} are given by $\mathbf{h}_i = [h_{1i} \ h_{2i} \ h_{3i}]^T$. The equation can be rewritten as $\mathbf{0}_{3 \times 1} = \mathbf{q} \times \mathbf{H}\mathbf{p}$ by a cross product, that is

$$\mathbf{0}_{3 \times 1} = \begin{bmatrix} \mathbf{0}_{1 \times 3} & -\mathbf{p}^T & v\mathbf{p}^T \\ \mathbf{p}^T & \mathbf{0}_{1 \times 3} & -u\mathbf{p}^T \\ -v\mathbf{p}^T & u\mathbf{p}^T & \mathbf{0}_{1 \times 3} \end{bmatrix} \begin{bmatrix} \mathbf{h}_1 \\ \mathbf{h}_2 \\ \mathbf{h}_3 \end{bmatrix} \quad (2)$$

where \mathbf{h}_i is the transposed matrix of the i -th row of \mathbf{H} . The 9×1 vector $[\mathbf{h}_1 \ \mathbf{h}_2 \ \mathbf{h}_3]^T$ is denoted as \mathbf{h} , \mathbf{p} is the points, u and v are the coordinates of points \mathbf{q} .

Only two rows in the above formula are linearly independent, so the first two rows are defined as

$$\mathbf{a}_i = \begin{bmatrix} \mathbf{0}_{1 \times 3} & -\mathbf{p}_i^T & v_i\mathbf{p}_i^T \\ \mathbf{p}_i^T & \mathbf{0}_{1 \times 3} & -u_i\mathbf{p}_i^T \end{bmatrix} \quad (3)$$

where $\mathbf{a}_i \in \mathbb{R}^{2 \times 9}$. Let \mathbf{a}_i be the first two rows of (2) computed for the i -th datum $\{\mathbf{p}_i, \mathbf{q}_i\}$.

Given N matching points, and let matrix $\mathbf{A} = [\mathbf{a}_1 \ \mathbf{a}_2 \ \dots \ \mathbf{a}_N]^T$. $\mathbf{A} \in \mathbb{R}^{2N \times 9}$ is obtained by stacking vertically \mathbf{a}_i for all i . We can estimate \mathbf{h} using

$$\mathbf{h} = \arg \min_{\mathbf{h}} \sum_{i=1}^N \|\mathbf{a}_i \mathbf{h}\|^2 = \arg \min_{\mathbf{h}} \|\mathbf{A}\mathbf{h}\|^2, \quad \|\mathbf{h}\|^2 = 1 \quad (4)$$

In [13], the method of using Gaussian weights to assign homography to any position in Moving DLT(MDLT) is

$$\mathbf{h}_* = \arg \min_{\mathbf{h}} \sum_{i=1}^N \left\| \omega_*^i \mathbf{a}_i \mathbf{h} \right\|^2 = \arg \min_{\mathbf{h}} \|\mathbf{W}_* \mathbf{A}\mathbf{h}\|^2 \quad (5)$$

where the weights $\{\omega_*^i\}_{i=1}^N$ are generated using the offset Gaussian. The $\omega_*^i = \max(\exp(-\|\mathbf{p}_* - \mathbf{p}_i\|^2 / \delta^2), \gamma)$,

$\gamma \in [0, 1]$. The δ is a scale parameter. The coordinates of arbitrary position are $\mathbf{p}_* = [x_* \ y_* \ 1]^T$. The coordinates of the i -th feature point are $\mathbf{p}_i = [x_i \ y_i \ 1]^T$. the weight matrix $\mathbf{W}_* \in \mathbb{R}^{2N \times 2N}$ is composed as

$$\mathbf{W}_* = \text{diag}([\omega_*^1 \ \omega_*^1 \ \omega_*^2 \ \omega_*^2 \ \dots \ \omega_*^N \ \omega_*^N]) \quad (6)$$

where the $\text{diag}()$ creates a diagonal matrix given a vector.

The local homography \mathbf{h}_* can be obtained by solving the smallest right singular vector of $\mathbf{W}_* \mathbf{A}$.

2) LOCAL WARPING

Most work uses a rectangular-based grid to align images. As shown in Figure 8(a), this method quickly treats multiple planes as coplanar, which seriously violates the premise of using homography. Therefore, the problem of ghosting in the stitched image is exacerbated. The recent warp, called TFA, triangulates the unit projection plane to construct a local transformation, as shown in Figure 9. Triangular segmentation is also easy to integrate heterogeneous images into cell images. Reasonable segmentation of non-coplanar pixels is the key to approaching the ideal condition of homography. Fortunately, superpixels can effectively achieve this goal. Based on this, we use the superpixel segmentation method to perform heterogeneous segmentation to approximate the constraints of homography. As shown in Figure 8(b), the proposed method also effectively reduces image cells, that is, reduces the amount of calculation of homography. Specifically, the multi-plane alignment method is divided into

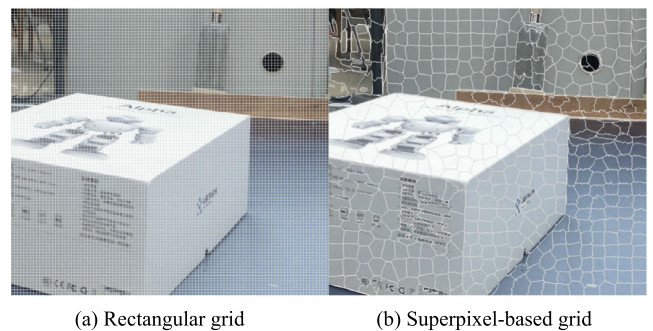


FIGURE 8. Different styles of grid segmentation methods.

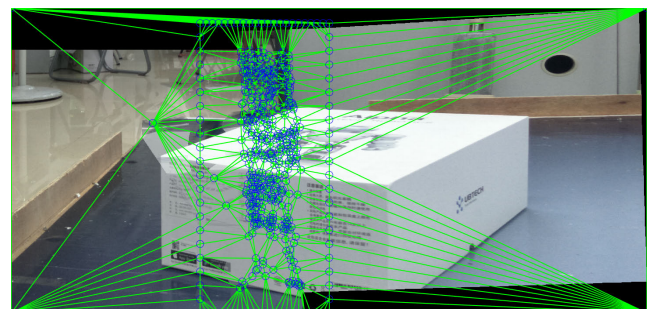


FIGURE 9. Triangulation segmentation [33].

three steps: First, segment the image to be spliced through the superpixel algorithm [44]; Second, the homography of irregular planes with more than 6 feature points (at least 4 pairs of points can be calculated) are calculated through DLT, while the homography of the remaining planes is calculated by MDLT. Third, use the estimated homography to project each surface to map the image onto the canvas. An arbitrary pixel at position \mathbf{x} in the source image I is warped to position \mathbf{x}_* in the target image I' . The image to be stitched can be warped onto the canvas at the same coordinates through equations (7) to (9).

$$\mathbf{x}'_* = \mathbf{H}\mathbf{x}_* \quad (7)$$

$$x'_{i,j} = \frac{h_{11}x_{i,j} + h_{12}y_{i,j} + h_{13}}{h_{31}x_{i,j} + h_{32}y_{i,j} + h_{33}} \quad (8)$$

$$y'_{i,j} = \frac{h_{21}x_{i,j} + h_{22}y_{i,j} + h_{23}}{h_{31}x_{i,j} + h_{32}y_{i,j} + h_{33}} \quad (9)$$

where $\mathbf{x}_* = [x_{i,j}, y_{i,j}, 1]^T$, $\mathbf{x}'_* = [x'_{i,j}, y'_{i,j}, 1]^T$. The $x_{i,j}$ and $y_{i,j}$ are the coordinates of arbitrary position (i, j) in the image. The positions mapped to the canvas are $x'_{i,j}$ and $y'_{i,j}$.

In practice, the number of pixels between the original image and the mapped image is not equal. That is, the size of the image before and after mapping is not consistent. To avoid empty pixels in the effective area of the map, we used MATLAB's built-in function "griddata" to fill in the empty pixels. Therefore, the target image I_2 can be mapped to the warped image I^t , that is, the canvas. And the reference image I_1 can be directly embedded into the canvas to obtain the warped image I^r .

In the last step, the warped images I^r and I^t are fused nonlinearly. The overlapping area (denoted as OLA) between warped images is an irregular two-dimensional image. Due to the rotation of the warped images, the pixel weighting is no longer in the horizontal direction. Inspired by ANAP [16], we use the following equation to map the two-dimensional coordinates in the OLA to the axis of rotation. This is similar to mapping the points inside the circle to the diameter.

$$L_{i,j} = \overrightarrow{PrPi,j} \cdot \overrightarrow{PrPt} \quad (10)$$

where the $L_{i,j}$ is the projection of the pixel at (i, j) on the rotation axis in the OLA. The $p_{i,j}$ is an arbitrary pixel coordinate in the OLA. The Pr and Pt are the center coordinates of the OLA in the warped images. $\overrightarrow{PrPi,j}$ and \overrightarrow{PrPt} are the vector to be projected and the axis of the rotation vector.

After the mapping is completed, as shown in equation (11), the linear weight is obtained by calculating the difference between the projection point of the pixel and the left boundary divided by the length of the OLA in the \overrightarrow{PrPt} direction.

$$\beta_{i,j} = \frac{L_{i,j} - L_{\min}}{L_{\max} - L_{\min}} \quad (11)$$

where the L_{\min} and L_{\max} are the left and right borders in the \overrightarrow{PrPt} direction.

The pixel weight matrix \mathbf{W}^t of I^t is calculated by equation (12) in the overlapping region of images I^r and I^t .

Specifically, the non-overlapping region weights are 1 in the image I^t . The sum of the weights of the images I^r and I^t at (i, j) is 1.

$$w_{i,j}^t = 0.5 - 0.5\cos(\pi \cdot \beta_{i,j}) \quad (12)$$

where the element of \mathbf{W}^t is $w_{i,j}^t$, which represents the weight at (i, j) in the overlapping region.

The elements of the matrix \mathbf{W}^t and the pixel of the image I^t are correspondingly multiplied to obtain the weight of each pixel. In the same way, the pixel weight of I^r is calculated. The stitched image can be obtained by adding the weighted warped image.

IV. EXPERIMENTAL RESULTS AND ANALYSIS

This section describes some experiments performed to evaluate the performance of the method on a series of challenging images. We compare our approach with the classical local homography methods [13], [16], [18] and other state-of-the-art stitching algorithms [27], [28], [33]. In our experiments, we used SIFT [35] and LSD [19] to detect the corresponding point and line features and matched the SIFT features through GMS [39], and HLM [41] matched the LSD features. Not only that, the proposed method combines GMM [44] and the normal distribution [28] to perform precise matching of SIFT and LSD features. Feature matching is done in the OpenCV library [45]. Finally, image stitching is completed by a multi-plane alignment method based on superpixel segmentation [44].

A. EXPERIMENTAL SETUP AND DATASETS

We use the source code provided by the authors, and the parameter settings follow the recommendations of the corresponding paper. If a range of values is provided, the parameter with the best effect is selected. Code is implemented in OpenCV 3.4.5 and Matlab 2017 on a desktop PC with Intel i7 3GHz CPU and 24GB memory for our method.

We compared six methods on a series of publicly available image pairs and additional images collected by us. The compared methods include APAP [13], ANAP [16], GSP [18], REW [27] and AAAP [28] and TFA [33]. Due to space limitations, only a few results can be shown here. More comparison results of overall performance from the dataset are available in the supplementary material. series of challenging images from various data sets were tested to evaluate the performance of the proposed method.

B. COMPARISON OF STITCHING QUALITY

The visual effects of stitched images and objective quality assessment indicators are often used to measure the performance of the method.

1) SUBJECTIVE EVALUATION

Stitched Image Comparison: Figure 10 shows the results of comparing our method with six methods in 2 challenging cases. The input images are placed in the first row to compare

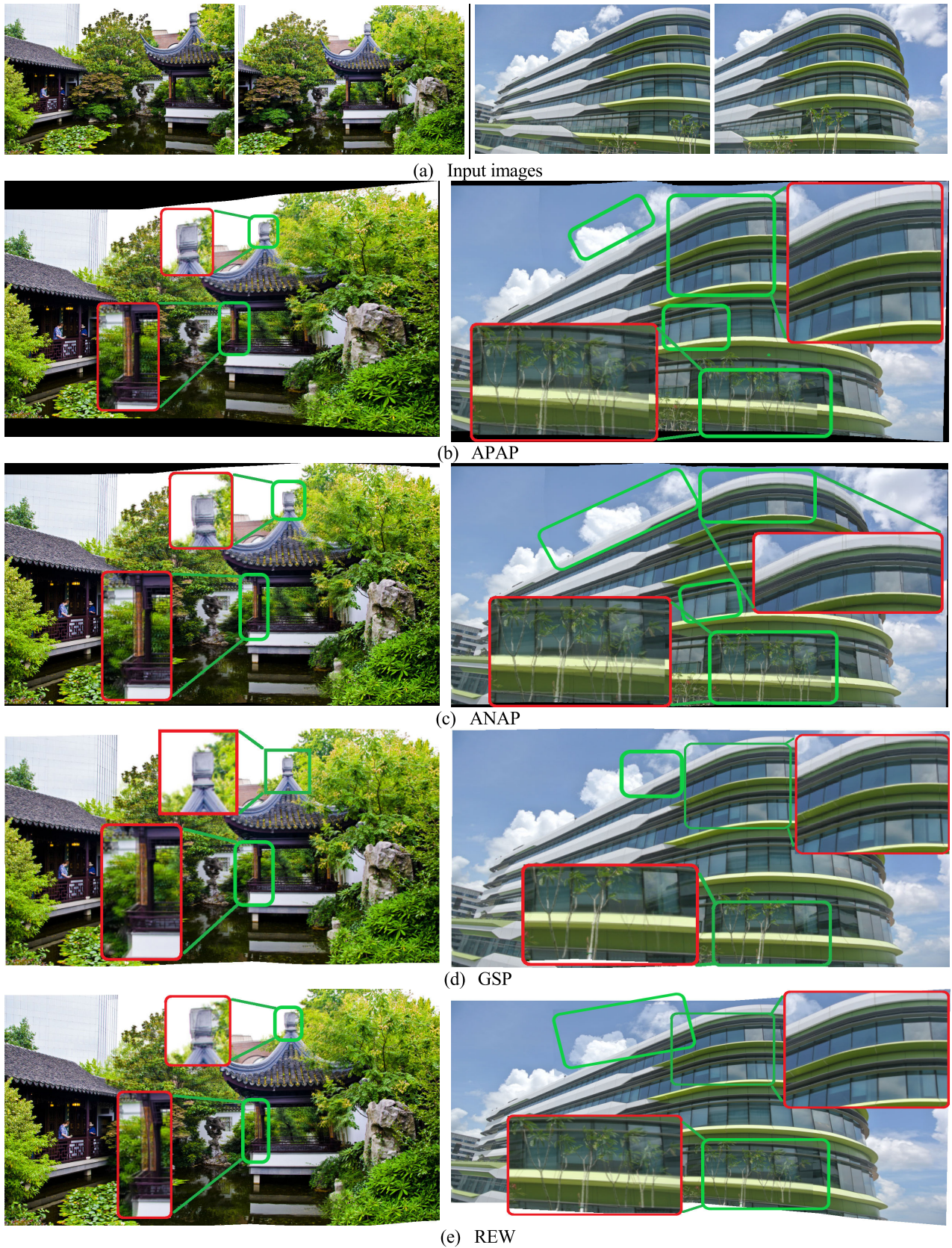


FIGURE 10. Comparison of stitching quality by the APAP [13], ANAP [16], GSP [18], REW [27], AAAP [28], TFA [33] and our approach on the garden [25] and building [26] scene.

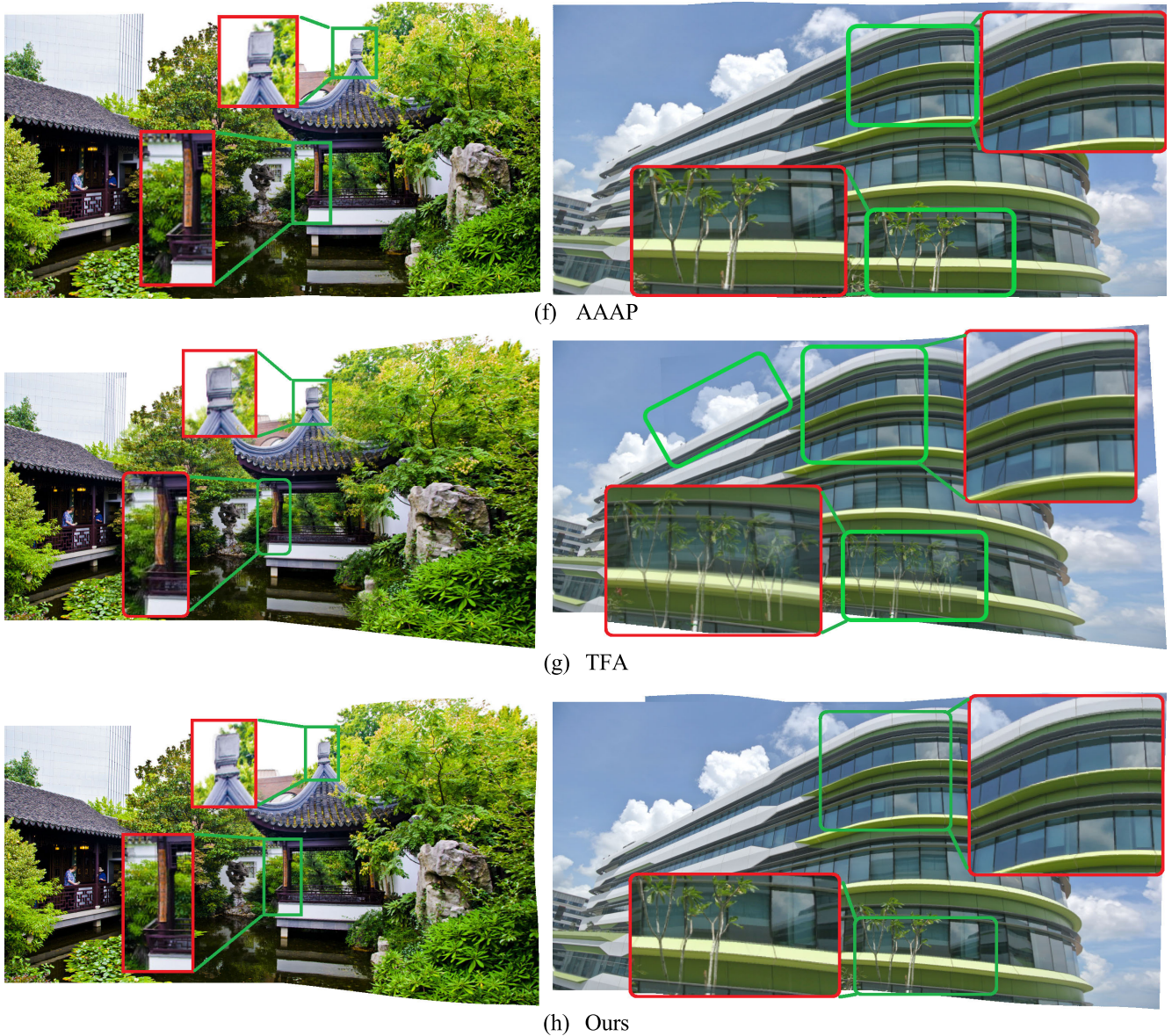


FIGURE 10. (Continued.) Comparison of stitching quality by the APAP [13], ANAP [16], GSP [18], REW [27], AAAP [28], TFA [33] and our approach on the garden [25] and building [26] scene.

the stitching result easily. The results of different methods are represented in rows, and the distorted area of each result image is highlighted with the rectangular box. Furthermore, to facilitate the observation, we mosaic the distorted, partially enlarged image in the resulting image.

We first analyze the results of the garden case. It can be observed from the test set on the left of Figure 10 that the top of the pavilion and the pillars are prone to ghosting. From the test set on the left side of Figure 10, it can be observed that the top of the pavilion and the pillars are prone to lose. Among them (b), (c), and (e), there are two prominent ghost images and distortions. The pillars in (d) and (g) show prominent ghost images, but our work (including (f)) does not show prominent ghost images or distortions.

For another parallax image shown in the right column of figure 10, it is obvious that the misalignment problem is extremely serious for methods other than the proposed method. In (b) and (c), there are 4 obvious ghost images and distortions (including white clouds, buildings, trees, etc.). APAP and ANAP are difficult to deal with large parallax and moving objects, which seriously affects the image quality. In (d), (e), and (f), the ghosting at the building has been resolved, but the ghosting at the white clouds and trees has not been removed. The TFA algorithm's effect is not good enough on this test chart, and there are several prominent ghost images. Furthermore, the result of our method looks good visually. It can successfully handle the misalignment issue.

APAP is a representative method for processing parallax images by the local homography. ANAP combines local homography with optimal global similarity to enhance the naturalness of the image. In addition, Recent warps such as GSP, REW, and AAAP use global similarity prior and global deformation constraints image warping, respectively. The recent warping TFA has taken a different approach, using triangular segmentation instead of rectangular segmentation. These excellent algorithms provide us with a wealth of contrast materials.

In summary, although APAP based only on the grid improves the alignment ability to a certain extent, it still cannot solve the large parallax image. Through the constraints of similar transformation, ANAP improves the stitching effect of images. But there are more ghosts. GSP also improves the effect of image alignment by calculating the best rotation angle and scale of the image. REW and AAAP achieve the purpose of improving alignment accuracy through additional deviation correction methods. For TFA based on triangle segmentation, the absence of constraints has improved the effect of image stitching. This is worthy of further study. The proposed method continues this idea, based on superpixel segmentation to separate each plane and obtain a more accurate transformation model. Finally, the projection deviation caused by parallax is improved.

2) OBJECTIVE EVALUATION

Alignment Accuracy Comparison: The matching quality of feature points is an important indicator to measure image stitching. In general, the more matches, the more robust the alignment accuracy. Table 1 shows the number of matching pairs obtained by different matching strategies. Combining the content of Figure 3 and the data in Table 1, it can be intuitively explained that the features acquired based on the RANSAC method are fewer (there are a few mismatches in the results). The ORB-based GMS has acquired more feature

point pairs, but it also contains some mismatches. It can be seen from Table 1 that the number of endpoints of the line segment is considerable, and the number of features obtained by RANSAC is mutually beneficial. These endpoints are potential matching points, which can enrich the matching set. The endpoint of the introduced line feature is used as the matching subset. Even if some mismatches are eliminated, the method in this paper still obtains more and effective feature point pairs. The proposed method has advantages in obtaining more accurate matches. On the other hand, we use SIFT descriptors for feature point extraction, which increases the base of feature matching and effectively improves features' richness.

To accurately reflect the alignment accuracy of the proposed method, the following formulas are used to calculate the cumulative sum of absolute deviations in the x and y directions, respectively.

$$SUM_{adx} = \sum_{i=1}^N |x'_i - x_i| \tag{13}$$

$$SUM_{ady} = \sum_{i=1}^N |y'_i - y_i| \tag{14}$$

where SUM_{adx} and SUM_{ady} are the cumulative sum of the absolute deviations in the x and y directions. x'_i and x_i are the x coordinates of the i -th pair of mapping points and matching points. y'_i and y_i are the y coordinates of the i -th pair of mapping points and matching points.

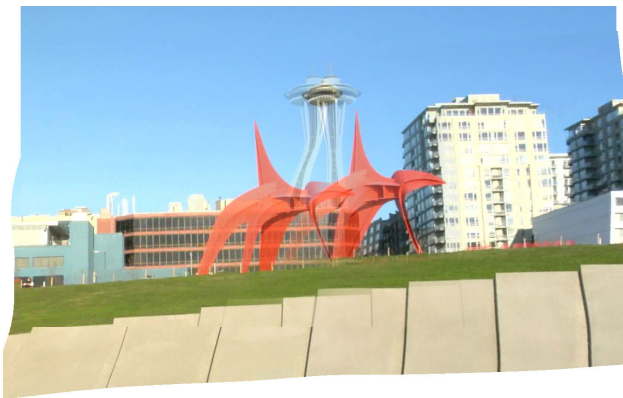
ANAP based on RANSAC is a representative of traditional matching strategies. MVPC eliminates mismatches by combining local homography with a fixed threshold. REW refines features through global homography and Gaussian distribution. AAAP combines local homography and Gaussian distribution to deal with mismatches. Different strategies have achieved different results, which provides us with a lot of experimental data.

TABLE 1. Number of matching features of different algorithms (in pairs).

| Database | SIFT+RANSAC[16] | ORB+GMS[39] | Ours/pair | |
|---------------|-----------------|-------------|-----------------------|---------|
| | Matches | Matches | Endpoints of the line | Matches |
| Box | 507 | 1414 | 293 | 1526 |
| Temple[11] | 415 | 3214 | 109 | 2705 |
| wall[4] | 791 | 2765 | 527 | 3136 |
| park[15] | 1335 | 1638 | 372 | 2773 |
| round[16] | 900 | 1608 | 263 | 2695 |
| seaport[16] | 497 | 4140 | 451 | 4648 |
| chessgirl[12] | 583 | 3228 | 289 | 3413 |
| paint | 621 | 1289 | 492 | 1918 |
| 24[26] | 855 | 2787 | 168 | 3219 |

TABLE 2. Accumulated projection deviation in the x and y directions. This indicator is an intuitive manifestation of the accuracy of feature alignment.

| Database | APDiTxD | | | | | APDiTyD | | | | |
|----------------------|-----------|-----------|----------|-----------|---------|-----------|-----------|----------|-----------|---------|
| | ANAP [16] | MVPC [17] | REW [27] | AAAP [28] | Ours | ANAP [16] | MVPC [17] | REW [27] | AAAP [28] | Ours |
| <i>building</i> [16] | 886.24 | 406.50 | 600.07 | 394.90 | 350.23 | 1715.71 | 682.40 | 1334.06 | 652.95 | 605.11 |
| <i>castle</i> [26] | 1673.43 | 498.16 | 1362.97 | 481.11 | 460.5 | 561.08 | 237.05 | 477.51 | 219.65 | 110.3 |
| <i>doll</i> [25] | 12989.61 | 4931.06 | 10277.83 | 4853.11 | 4635.15 | 2115.57 | 769.70 | 1177.39 | 735.17 | 698.19 |
| <i>forest</i> [26] | 134.84 | 82.07 | 77.03 | 62.45 | 55.64 | 63.36 | 48.57 | 42.45 | 39.39 | 37.98 |
| <i>garden</i> [13] | 8447.63 | 2681.92 | 4000.85 | 2387.74 | 2286.4 | 3804.95 | 998.78 | 2113.21 | 956.81 | 955.85 |
| <i>garden</i> [15] | 3915.14 | 1205.58 | 1926.83 | 1203.15 | 1189.5 | 5575.66 | 1112.92 | 3296.93 | 1040.72 | 1000.95 |
| <i>temple</i> [13] | 444.71 | 177.26 | 353.45 | 162.46 | 123.85 | 290.05 | 105.73 | 224.18 | 85.68 | 64.5 |
| <i>Theater</i> [27] | 31984.10 | 16706.95 | 24525.03 | 11553.28 | 9846.24 | 5352.10 | 1953.96 | 3513.98 | 1855.03 | 1525.9 |
| <i>street</i> [25] | 944.99 | 413.50 | 498.21 | 383.34 | 348.78 | 794.63 | 358.75 | 527.86 | 319.12 | 315.75 |
| <i>Uffizi</i> [18] | 18970.43 | 8736.26 | 13467.11 | 8580.94 | 8552.1 | 9871.19 | 3972.63 | 5297.13 | 3959.86 | 3594.97 |



(a) Ghosting caused by large parallax



(b) Ghosting caused by motion

FIGURE 11. Failure examples. The proposed method will fail in some scenes, such as sports and large parallax.

We select the algorithm with the least number of feature sets in each group as the statistical standard number, and other algorithms take their respective subsets to unify the number of feature points to achieve the purpose of a single variable comparison. Calculate the absolute sum of the mapping deviations of the feature points in the x and y directions to obtain Table 2.

We can see from Table 2 that the projection error of ANAP is the largest, followed by REW. They have larger projection deviations in the horizontal and vertical directions, while the projection errors of MVPC and AAAP are much smaller.

What is more, the projection error obtained from this work has been further reduced.

In 10 experiments with large parallax, it is obvious that the results obtained by the proposed method are always smaller than those of the listed methods. The traditional matching strategy [16] inevitably retains some outliers in the iterative process. MVPC uses a constant threshold to eliminate outliers, which are prone to error rejection or retention. Moreover, a constant threshold also brings limitations to matching, which more or less restricts certain matching judgments. REW and AAAP use “SIFT + RANSAC” for the initial matching of feature points. Then a combination of homography and normal distribution is used to eliminate mismatches effectively. Finally, the matching error is further reduced, but the matching points obtained are not sufficient. In terms of the types of image features, none of them considers the straight-line features of the image, although they have noticed the important role of local transformation in feature matching. We know that the straight-line feature can do the addition operation for the feature set, and the local transformation can only delete the potential mismatches in the feature set, that is, the subtraction operation. Therefore, the introduction of line features and local classification can enrich the feature set and improve the matching accuracy. The proposed method introduces line features, split plane calculation homography, and GMS-based matching strategy, and proposes an optimized matching method to make up for the shortcomings of the matching method in the previous stage of work and further improves the accuracy of image mapping. Finally, uniform distribution and a considerable number of matching pairs are obtained. This method achieved the slightest projection error in Table 2.

C. FAILURE CASES

Our proposed warp could fail if the parallax is too large. In addition, when there are moving people or objects in the overlapping area, it will produce more obvious ghosting. Two failure examples are shown in Figure 11. If the viewing angle is too large, the scene structure will change greatly. The appearance of moving objects also increases the difficulty of

image fusion. Therefore, only relying on homography to deal with these scenes is less effective.

V. CONCLUSION

In this paper, we propose a novel stitching method to solve the problem of local misalignment. We introduce line features to enrich image matching. Not only that, we introduce superpixel segmentation in the feature matching and local warping stages. In addition, irregular plane segmentation can effectively avoid the heterogeneous objects sticking in the same image cell and fit the homography coplanar condition as much as possible. The experimental results show that the proposed method can accurately align the image and outperform some state-of-the-art warps from both qualitative and quantitative aspects. As future work, we will combine the feature registration research based on deep learning to optimize the extraction of image features. We will also use linear features for content protection research to prevent objects in the image from being bent during the image deformation process.

REFERENCES

- [1] T. Xiang, G.-S. Xia, L. Zhang, and N. Huang, "Locally warping-based image stitching by imposing line constraints," in *Proc. 23rd Int. Conf. Pattern Recognit. (ICPR)*, Dec. 2016, pp. 4178–4183.
- [2] F. Zhang and F. Liu, "Casual stereoscopic panorama stitching," in *Proc. IEEE Conf. Comput. Vis. Pattern Recognit. (CVPR)*, Jun. 2015, pp. 2002–2010.
- [3] J. Zheng, Z. Zhang, Q. Tao, K. Shen, and Y. Wang, "An accurate multi-row panorama generation using multi-point joint stitching," *IEEE Access*, vol. 6, pp. 27827–27839, 2018.
- [4] H.-Y. Shum, K.-T. Ng, and S.-C. Chan, "A virtual reality system using the concentric mosaic: Construction, rendering, and data compression," *IEEE Trans. Multimedia*, vol. 7, no. 1, pp. 85–95, Feb. 2005.
- [5] K. Y. Lee and J. Y. Sim, "Stitching for multi-view videos with large parallax based on adaptive pixel warping," *IEEE Access*, vol. 6, pp. 26904–26917, 2018.
- [6] R. Szeliski, "Image alignment and stitching: A tutorial," *Found. Trends Comput. Graph. Vis.*, vol. 2, no. 1, pp. 1–104, 2006.
- [7] A. Levin, A. Zomet, S. Peleg, and Y. Weiss, "Seamless image stitching in the gradient domain," in *Proc. Eur. Conf. Comput. Vis. (ECCV)*, 2004, pp. 377–389.
- [8] F. Liu, M. Gleicher, H. Jin, and A. Agarwala, "Content-preserving warps for 3D video stabilization," *ACM Trans. Graph.*, vol. 28, pp. 223–231, Jul. 2009.
- [9] N. Li, Y. Xu, and C. Wang, "Quasi-homography warps in image stitching," *IEEE Trans. Multimedia*, vol. 20, no. 6, pp. 1365–1375, Jun. 2018.
- [10] M. Brown and D. G. Lowe, "Automatic panoramic image stitching using invariant features," *Int. J. Comput. Vis.*, vol. 74, no. 1, pp. 59–73, Aug. 2007.
- [11] J. Gao, S. J. Kim, and M. S. Brown, "Constructing image panoramas using dual-homography warping," in *Proc. IEEE Conf. Comput. Vis. Pattern Recogn. (CVPR)*, Jun. 2011, pp. 49–56.
- [12] W.-Y. Lin, S. Liu, Y. Matsushita, T.-T. Ng, and L.-F. Cheong, "Smoothly varying affine stitching," in *Proc. IEEE Conf. Comput. Vis. Pattern Recogn. (CVPR)*, Jun. 2011, pp. 345–352.
- [13] J. Zaragoza, T.-J. Chin, M. S. Brown, and D. Suter, "As-projective-as-possible image stitching with moving DLT," in *Proc. IEEE Conf. Comput. Vis. Pattern Recogn. (CVPR)*, Jun. 2013, pp. 2339–2346.
- [14] Z. Lou and T. Gevers, "Image alignment by piecewise planar region matching," *IEEE Trans. Multimedia*, vol. 16, no. 7, pp. 2052–2061, Nov. 2014.
- [15] C.-H. Chang, Y. Sato, and Y.-Y. Chuang, "Shape-preserving half-projective warps for image stitching," in *Proc. IEEE Conf. Comput. Vis. Pattern Recognit.*, Jun. 2014, pp. 3254–3261.
- [16] C.-C. Lin, S. U. Pankanti, K. N. Ramamurthy, and A. Y. Aravkin, "Adaptive as-natural-as-possible image stitching," in *Proc. IEEE Conf. Comput. Vis. Pattern Recognit. (CVPR)*, Jun. 2015, pp. 1155–1163.
- [17] G. Zhang, Y. He, W. Chen, J. Jia, and H. Bao, "Multi-viewpoint panorama construction with wide-baseline images," *IEEE Trans. Image Process.*, vol. 25, no. 7, pp. 3099–3111, Jul. 2016.
- [18] Y.-S. Chen and Y.-Y. Chuang, "Natural image stitching with the global similarity prior," in *Proc. Eur. Conf. Comput. Vis. (ECCV)*, 2016, pp. 186–201.
- [19] R. G. von Gioi, J. Jakubowicz, J.-M. Morel, and G. Randall, "LSD: A fast line segment detector with a false detection control," *IEEE Trans. Pattern Anal. Mach. Intell.*, vol. 32, no. 4, pp. 722–732, Apr. 2010.
- [20] L. Zhang and R. Koch, "An efficient and robust line segment matching approach based on LBD descriptor and pairwise geometric consistency," *J. Vis. Commun. Image Represent.*, vol. 24, no. 7, pp. 794–805, 2013.
- [21] S. Li, L. Yuan, J. Sun, and L. Quan, "Dual-feature warping-based motion model estimation," in *Proc. IEEE Int. Conf. Comput. Vis. (ICCV)*, Dec. 2015, pp. 4283–4291.
- [22] K. Joo, N. Kim, T.-H. Oh, and I. S. Kweon, "Line meets as-projective-as-possible image stitching with moving DLT," in *Proc. IEEE Int. Conf. Image Process. (ICIP)*, Sep. 2015, pp. 1175–1179.
- [23] T.-Z. Xiang, G.-S. Xia, X. Bai, and L. Zhang, "Image stitching by line-guided local warping with global similarity constraint," *Pattern Recognit.*, vol. 83, pp. 481–497, Nov. 2018.
- [24] J. Gao, L. Yu, T.-J. Chin, and M. Brown, "Seam-driven image stitching," *Eurographics*, vol. 2013, pp. 45–48, May 2013.
- [25] F. Zhang and F. Liu, "Parallax-tolerant image stitching," in *Proc. IEEE Conf. Comput. Vis. Pattern Recognit.*, Jun. 2014, pp. 3262–3269.
- [26] K. Lin, N. Jiang, L.-F. Cheong, M. Do, and J. Lu, "SEAGULL: Seam-guided local alignment for parallax-tolerant image stitching," in *Proc. Eur. Conf. Comput. Vis. (ECCV)*, 2016, pp. 370–385.
- [27] J. Li, Z. Wang, S. Lai, Y. Zhai, and M. Zhang, "Parallax-tolerant image stitching based on robust elastic warping," *IEEE Trans. Multimedia*, vol. 20, no. 7, pp. 1672–1687, Jul. 2018.
- [28] J. Li, P. Jiang, S. Song, H. Xia, and M. Jiang, "As-aligned-as-possible image stitching based on deviation-corrected warping with global similarity constraints," *IEEE Access*, vol. 7, pp. 156603–156611, 2019.
- [29] F. L. Bookstein, "Principal warps: Thin-plate splines and the decomposition of deformations," *IEEE Trans. Pattern Anal. Mach. Intell.*, vol. 11, no. 6, pp. 567–585, Jun. 1989.
- [30] H. Zhou, Y. Kuang, Z. Yu, S. Ren, Y. Zhang, T. Lu, and J. Ma, "Image deformation with vector-field interpolation based on MRLS-TPS," *IEEE Access*, vol. 6, pp. 75886–75898, 2018.
- [31] T. Liao and N. Li, "Single-perspective warps in natural image stitching," *IEEE Trans. Image Process.*, vol. 29, pp. 724–735, 2020.
- [32] T. Xiang, G. Xia, and L. Zhang, "Image stitching using smoothly planar homography," in *Proc. Chin. Conf. Pattern Recogn.*, 2018, pp. 524–536.
- [33] J. Li, B. Deng, R. Tang, Z. Wang, and Y. Yan, "Local-adaptive image alignment based on triangular facet approximation," *IEEE Trans. Image Process.*, vol. 29, pp. 2356–2369, 2020.
- [34] S. M. Seitz and J. Kim, "Multiperspective imaging," *IEEE Comput. Graph. Appl.*, vol. 23, no. 6, pp. 16–19, Nov. 2003.
- [35] D. G. Lowe, "Distinctive image features from scale-invariant keypoints," *Int. J. Comput. Vis.*, vol. 60, no. 2, pp. 91–110, Feb. 2004.
- [36] H. Bay, T. Tuytelaars, and L. V. Gool, "SURF: Speeded up robust features," in *Proc. Eur. Conf. Comput. Vis. (ECCV)*, 2006, pp. 404–417.
- [37] E. Rublee, V. Rabaud, K. Konolige, and G. Bradski, "ORB: An efficient alternative to SIFT or SURF," in *Proc. Int. Conf. Comput. Vis.*, Nov. 2011, pp. 2564–2571.
- [38] E. Rosten, R. Porter, and T. Drummond, "Faster and better: A machine learning approach to corner detection," *IEEE Trans. Pattern Anal. Mach. Intell.*, vol. 32, no. 1, pp. 105–119, Jan. 2010.
- [39] J. Bian, W.-Y. Lin, Y. Matsushita, S.-K. Yeung, T.-D. Nguyen, and M.-M. Cheng, "GMS: Grid-based motion statistics for fast, ultra-robust feature correspondence," in *Proc. IEEE Conf. Comput. Vis. Pattern Recognit. (CVPR)*, Jul. 2017, pp. 4181–4190.
- [40] Q. Jia, X. Gao, X. Fan, Z. Luo, H. Li, and Z. Chen, "Novel coplanar line-points invariants for robust line matching across views," in *Proc. Eur. Conf. Comput. Vis. (ECCV)*, 2016, pp. 599–611.

- [41] K. Li, J. Yao, X. Lu, L. Li, and Z. Zhang, "Hierarchical line matching based on line-junction-line structure descriptor and local homography estimation," *Neurocomputing*, vol. 184, pp. 207–220, Apr. 2016.
- [42] N. Li, T. Liao, and C. Wang, "Perception-based seam cutting for image stitching," *Signal, Image Video Process.*, vol. 12, no. 5, pp. 967–974, Jul. 2018.
- [43] O. R. Chum and J. Matas, "Optimal randomized RANSAC," *IEEE Trans. Pattern Anal. Mach. Intell.*, vol. 30, no. 8, pp. 1472–1482, Aug. 2008.
- [44] Z. Ban, J. Liu, and L. Cao, "Supersixel segmentation using Gaussian mixture model," *IEEE Trans. Image Process.*, vol. 27, no. 8, pp. 4105–4117, Aug. 2018.
- [45] G. Bradski, "The openCV library," *Dr. Dobbs's J. Softw. Tools*, vol. 25, no. 11, pp. 120–123, 2000.



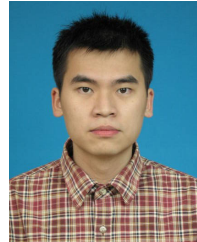
JIALIANG LI was born in Henan, China, in 1995. He received the B.S. degree from the Henan Institute of Science and Technology, Xinxiang, China, in 2017, and the M.S. degree from Guangxi Normal University, Guilin, China, in 2020. He currently teaches with the College of Artificial Intelligence, Zhejiang Post and Telecommunication College. His current research interests include computer vision, image stitching, and video mosaics.



DONG WU received the B.S. degree from the Memorial University of Newfoundland, St. John's, Canada, in 2015, and the M.S. degree from Monash University, in 2019. He currently teaches with the College of Artificial Intelligence, Zhejiang Post and Telecommunication College. His current research interests include computer vision, deep learning, and big data.



PINQUN JIANG received the Ph.D. degree in the doctorate in theoretical physics from the University of Science and Technology of China, in 2005. He is currently an Associate Professor with the Department of Electronic Science and Technology, College of Electronic Engineering, Guangxi Normal University. His research interests include analog integrated circuit design, artificial intelligence, and machine vision.



ZILI LI received the Ph.D. degree from the Electronic Information School, Wuhan University, in 2010. He is currently an Associate Professor with the Department of Electronic Science and Technology, College of Electronic Engineering, Guangxi Normal University. His research interests include digital signal processing, radar signal processing, and machine vision.



SHUXIANG SONG received the Ph.D. degree from the Department of Electronic and Information Engineering, Huazhong University of Science and Technology, Wuhan, China. He is currently a Full Professor with Guangxi Normal University. His current research interests include intelligent detection, automatic control, and signal and image processing.

...